Applied Catalysis B: Environmental 258 (2019) 117972

Contents lists available at ScienceDirect

Applied Catalysis B: Environmental

journal homepage: www.elsevier.com/locate/apcatb

Poly(ionic liquid)-supported gold and ruthenium nanoparticles toward the catalytic wet air oxidation of ammonia to nitrogen under mild conditions

Hengjun Gai, Caiyun Zhong, Xiaofeng Liu, Lin Qiao, Xiaowei Zhang, Meng Xiao, Hongbing Song*

State Key Laboratory Base for Eco-Chemical Engineering in College of Chemical Engineering, Qingdao University of Science and Technology, Zhengzhou Road No.53, Qingdao 266042, China

ARTICLE INFO

Keywords:
Poly(ionic liquid)s
Metal nanoparticles
Catalytic wet air oxidation
Ammonia

ABSTRACT

In this study, gold (Au) and ruthenium (Ru) atoms were successfully anchored onto poly(ionic liquid)s (PILs) containing imidazolium-based ionic liquids (ILs) and ethylene glycol dimethacrylate (EGDMA), thereby yielding efficient heterogeneous encapsulated metal catalysts Au/PILs and Ru/PILs for the catalytic wet air oxidation (CWAO) of ammonia. The as-synthesized catalysts were characterized via X-ray photoelectron spectroscopy, scanning electron microscopy mapping, and transmission electron microscopy. The results indicated that the metal nanoparticles with uniform distribution could be produced due to the interactions between the supports and the metals, leading to an excellent catalytic property for catalysts. These catalysts exhibited good activity and stability for the CWAO of ammonia with high selectivity to nitrogen (N_2) under mild conditions. Compared with the Au/PILs catalyst giving 65.8% conversion with a selectivity of 99%, the Ru/PILs catalyst provided 86.5% ammonia conversion with 95% selectivity to N_2 under 1 MPa at 160 °C in 4 h.

1. Introduction

During coal gasification and petroleum refining, ammonia is transferred to air and water, thereby causing serious atmosphere and water pollution. Ammonia in wastewater not only causes serious eutrophication problems but also has toxic side effects on aquatic organisms and humans. The oxidation of ammonia to nitrogen oxides (NO and NO_2) could contribute to a series of environmental problems, such as acid rain and photochemical smog, which pose harm to human health [1–3]. Therefore, the pollution control and treatment of ammonia have elicited widespread attention.

Different treatment methods have been adopted to treat ammonia-containing wastewater due to the varying concentrations of ammonia in wastewater. At present, the primary treatment methods include air stripping [4], steam stripping [5], breakpoint chlorination [6,7], nitrification-denitrification [8,9], and catalytic wet air oxidation (CWAO) [10,11]. Among these methods, air stripping has been banned because it produces large amounts of ammonia slip. Steam stripping is suitable for treating high-concentration ammonia-containing wastewater but is uneconomical for treating low-concentration ammonia-containing wastewater. In breakpoint chlorination, the residual chloride produced in the process can increase the corrosion of subsequent treatment equipment. For nitrification-denitrification, the long technological process requires a large area and it is easily affected by climate, thereby resulting in unstable operation. Considering that ammonia is produced in the coal chemical and petroleum refining processes, the use of CWAO is speculated to be economically advantageous because coal chemical and petroleum refining plants have a complete air separation unit and sufficient heat source. Qin et al. [11] reported that the catalyst of 3% Ru/Al_2O_3 performed at 497 °C for the CWAO of ammonia, whereas Lin et al. [12] indicated that the catalyst of Au/Al_2O_3 worked at 230 °C for the selective catalytic oxidation of NH_3. These findings indicate that ruthenium (Ru) and gold (Au) can function as active metals for the CWAO of ammonia.

The support is another an important parameter obtaining stable and efficient supported metal nanoparticles (NPs) [13,14]. On the basis of a previous study, a support can be modified to allow certain interactions to occur between the catalytic support and the active metal to promote the dispersion and stabilization of the active metal on the support [15,16]. In this context, poly(ionic liquid)s (PILs) are selected as support. These materials maintain some properties of ionic liquids (ILs) and polymers, including an adjustable pore structure, a multifunctional organic framework (specific functional groups), and excellent ionic conductivity (ion sites) [17–20]. The actual performance of PILs is closely related to their pore structure, which has promoted the development of various pore formation strategies [21–23]. High-performance catalysts can be manufactured by controlling the size, shape, composition, and structure of active metals [24,25]. This method is

* Corresponding author.
E-mail address: cehbsong@qust.edu.cn (H. Song).

https://doi.org/10.1016/j.apcatb.2019.117972
Received 1 March 2019; Received in revised form 14 July 2019; Accepted 16 July 2019
Available online 18 July 2019
0926-3373/

feasible because ion sites on PILs can provide the homogeneous dispersion of active metal precursors at the molecular level, thereby facilitating the fine control of active metal formation and structure in the successive reduction. Although several metals NPs on PILs have been adopted as heterogeneous catalysts, the use of such catalysts in CWAO of ammonia has not yet been reported.

According to related literature reports, in the study of the oxidation of benzene to biphenyl, it was found that the −COOH group and $-SO_3H$ could interact with palladium, so that palladium was immobilized on the catalyst supports [15,26]. In the study of chitin used as the catalyst support, it has been demonstrated that a lone pair of electron nitrogen on acetamide and a hydroxyl group can be used as a chelation site for the metals, thereby effectively immobilizing noble metals such as palladium nanoparticles [27,28]. Therefore, in our work, ILs containing imidazolium ring were chosen as monomers of polymers, ethylene glycol dimethacrylate (EGDMA) containing −COO− was chosen as a crosslinking agent to copolymerize with ILs, and NTf_2 containing −S═O group was chosen as anions of ILs.

In the study, PILs with different spatial structures were used as support for catalysts, and Au and Ru were selected as active metals. Characterizations, including Fourier transform infrared spectroscopy (FT-IR), Brunauer–Emmett–Teller (BET), X-ray photoelectron spectroscopy (XPS), thermogravimetric (TG) analysis, transmission electron microscopy (TEM), scanning electron microscopy (SEM), and SEM mapping were performed to evaluate the relationship between the catalytic performance and structure of PILs in details.

2. Experimental

2.1. Materials

Bromoethane, 1,2-dibromoethane, 1-vinylimidazole, ethylene glycol dimethacrylate (EGDMA), and 2,2-Azobisisobutyronitrile (AIBN) were purchased from Aladdin Internet Reagent Database Inc. (Shanghai, China). Methanol, ethyl acetate, potassium hexafluorophosphate, sodium borohydride, chloroauric acid ($HAuCl_4{\cdot}4H_2O$) and ruthenium (III) chloride ($RuCl_3{\cdot}3H_2O$) were obtained from Sinopharm Chemical Reagent Co. Ltd. (Shanghai, China). Bis(trifluoromethanesulfonyl)imide lithium salt ($LiNTf_2$) was purchased from Sigma Aldrich. Ionic liquids monomers [EVim]Br [29] and [E(Vim)$_2$][Br$_2$] [30] are prepared according to reference methods.

2.2. Synthesis of supports

2.2.1. Ionic liquids (ILs)

Bromoethane (5.45 g, 50 mmol) was dripped into 1-vinylimidazole (3.76 g, 40 mol) solution in an ice bath. A mixture of 1-vinylimidazole and bromoethane was stirred at room temperature for 28 h. Then washed with anhydrous ether and ethyl acetate, dried in vacuum overnight to get white IL crystal named [EVim]Br. The solid was dried at 40 °C for 24 h. For [E(Vim)$_2$][Br$_2$], the reactants are 1,2-dibromoethane (3.76 g, 20 mmol) and 1-vinylimidazole (3.76 g, 40 mmol), and the reaction temperature is 45 °C, and the reaction should be N_2/degas cycles. Other procedures are similar to [EVim]Br.

2.2.2. [EVim]Br

^{1}H NMR (400 MHz, d_6-DMSO): δ = 1.43 (m, 3 H), 4.21 (m, 2 H), 5.40 (m,1 H), 5.98 (m, 1 H), 7.30 (s, 1 H), 7.96 (s, 1 H), 8.21 (s, 1 H), 9.59 (s,1 H).

2.2.3. [E(Vim)$_2$][Br$_2$]

^{1}H NMR (400 MHz, d_6-DMSO): δ = 4.78 (s, 2 H), 5.44 (m, 1 H), 5.97 (m, 1 H), 7.33 (m, 1 H), 7.84 (s, 1 H), 8.22 (s, 1 H), 9.54 (s, 1 H).

2.2.4. Polymeric ionic liquid (PILs)

The polymeric procedure in this work is similar to Lu's work [31].

Table 1
The structure of the ILs and PILs.

Structure	Abbreviation
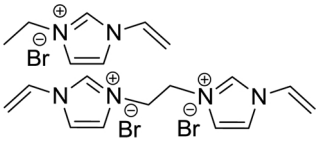	[EVim]Br
	[E(Vim)$_2$][Br$_2$]
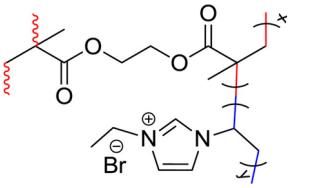	PILs-Br
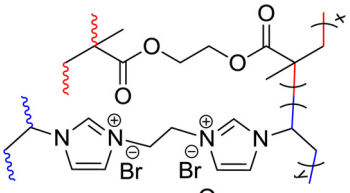	D-PILs-Br
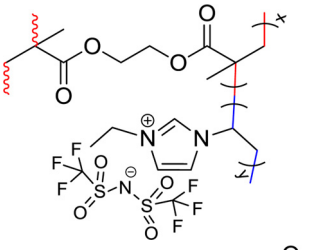	PILs-NTf$_2$
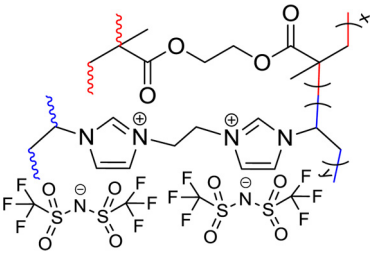	D-PILs-NTf$_2$

[EVim]Br (0.203 g, 1 mmol) was added to a 100 mL Schlenk flask and dispersed in 50 mL methanol by stirring for 15 min so that [EVim]Br dissolved completely in methanol. Then EGDMA (0.198 g, 1 mmol) and AIBN (0.006 g, 0.037 mmol) were added in the Schlenk flask. After N_2 − vacuum cycles, the mixture was heated and stirred in a thermostatically controlled oil bath at 70 °C for 20 h. The obtained poly(ionic liquids) named P([EVim]Br-EGDMA). Then the desired lithium salt $LiNTf_2$ was added to replace the Br^- anion with NTf_2^- anion. After stirring 24 h at room temperature, the mixture was filtered and washed by ethyl acetate. The ion exchange experiments were repeated three times. Finally, the product was dried in vacuum overnight at 40 °C and named as P([EVim][NTf$_2$]-EGDMA). Other PILs were prepared in a similar procedure, and the obtained P([EVim]Br-EGDMA), P([EVim][NTf$_2$]-EGDMA), P([E(Vim)$_2$][Br$_2$]-EGDMA) and P([E(Vim)$_2$][(NTf$_2$)$_2$]-EGDMA) were referred to as PILs-Br, PILs-NTf$_2$, D-PILs-Br and D-PILs-NTf$_2$, respectively. The structures of ILs and PILs are list in (Table 1).

2.3. Catalyst preparation

The chemical reduction method was used to produce catalysts, where PILs referred to the polymer supports, using $HAuCl_4{\cdot}4H_2O$ and $RuCl_3{\cdot}3H_2O$ as active metal precursors, respectively. Typically, 0.5 g PILs were added into 20 mL solution of $HAuCl_4{\cdot}4H_2O$ (containing the desired Au). The mixture was oscillated for 24 h using a constant

temperature water bath oscillator at room temperature. The mixture was filtered and washed with deionized water. Then desired $NaBH_4$ was added to reduce Au^{3+} to Au. After stirring 4 h at room temperature, the mixture was filtered and washed by deionized water. The solid was dried for 24 h at 40 °C. The obtained catalysts were denoted as Au/PILs. Catalysts containing Ru were made in the same way, and the obtained catalysts were denoted as Ru/PILs. The loading of Au or Ru on the support was 1 wt%. The actual content of Au or Ru on the support was calculated by ICP-MS, and the results were shown in Table S1.

2.4. Characterization

The FT-IR of the samples were obtained using a Bruker Tensor 27 FT-IR spectrometer. The nuclear magnetic resonance (^{1}H NMR) of the samples were collected by Bruker AVANCE III at 500 MHz. The morphologies and microstructures of catalysts and supports were observed by scanning electron microscopy (SEM, Sirion200, Philips, Netherlands) and transmission electron microscopy (TEM, JEOL, Japan). Thermogravimetric (TG, SDT Q600) analysis was adopted under air condition at a heating rate of 10 °C min^{-1} to analyze the thermal stability of PILs. The X-ray photoelectron spectra (XPS) of the samples were investigated by a Quantum 2000. The remaining metal in adsorption was measured by inductively coupled plasma mass spectrometry (ICP-MS, NexION2000). All the samples were degassed under vacuum for 20 h. The specific surface area and pore size distribution of PILs and catalysts were calculated by the Brunauer–Emmett–Teller (BET) and Barrett–Joyner–Halenda (BJH) method (ASAP 2020), respectively.

2.5. Apparatus and procedure

The reaction process of this work is similar to that of Li [32]. The reaction was carried out using a 25 mL reactor equipped with a thermostatic magnetic stirrer, and the reactor had a Teflon liner 2 mm thick inside to prevent corrosion of the reactor wall. Typically, 0.1 g of catalyst and 5 mL of a solution containing 1000 ppm ammonia were added to the reactor for each reaction. Qin et al. [11] reported that the reaction hardly proceeded in the acidic region, but completely reacted in the range of pH above 10, and the preferred pH range was approximately 11 to 12.3. Hence, the 2 M NaOH solution was used to adjust the pH of 1000 ppm ammonia. After the reactor was sealed, filled with a certain amount of oxygen. Finally, the reactor was heated to the desired temperature and reacted with a magnetic stirrer for 4 h. When the reaction was completed, the reactor was moved out from the heater and cooled to room temperature. The liquid samples and solid catalysts in the reactor were collected and filtered. In calculating the conversion of ammonia, the adsorption of ammonia by catalysts must be excluded to ensure the accuracy of the determination results. The process of eliminating adsorption interference in this work was as described below. The catalysts should be washed with H_2SO_4 solution three times, and the washing liquid and catalytic reaction solution were combined to determine the ammonia content. The concentration of ammonia-nitrogen in water was measured by TU-1810 UV–vis spectrophotometry according to HJ 535-2009, and the concentrations of NO_2^- and NO_3^- were determined by ion chromatography (DIONEX DX-120).

The ammonia conversion (X_{NH_3}) and nitrogen selectivity (S_{N_2}) were calculated as follows.

$$X_{NH_3} = \frac{C^0_{NH_3} - C_{NH_3}}{C^0_{NH_3}} \times 100\% \quad (1)$$

$$S_{N_2} = \left(1 - \frac{C_{NO_3^-} + C_{NO_2^-}}{C^0_{NH_3} - C_{NH_3}}\right) \times 100\% \quad (2)$$

Where the $C^0_{NH_3}$ and C_{NH_3} were the initial and final concentrations (in mmol·L^{-1}) of ammonia in the solution, respectively, $C_{NO_3^-}$ and $C_{NO_2^-}$ are the concentrations (in mmol·L^{-1}) of NO_3^- and NO_2^- in the solution after the reaction, respectively.

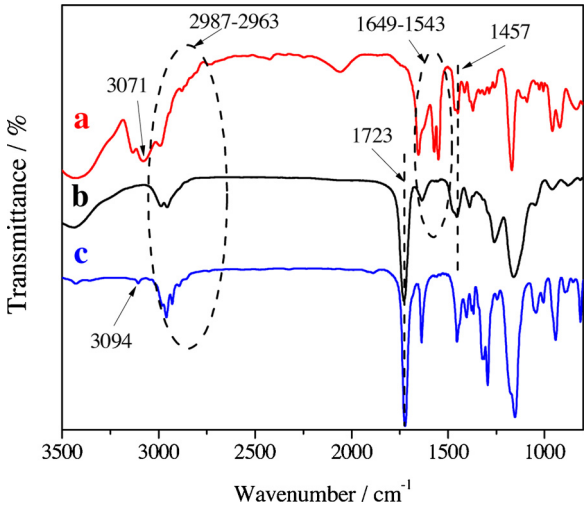

Fig. 1. FT-IR spectra of (a) [EVim]Br, (b) PILs-Br, (c) EGDMA.

3. Results and discussion

3.1. Characterization of supports and supported catalysts

Due to the similarity of the PILs involved in this paper, PILs-Br, PILs-NTf_2, Au/PILs-NTf_2 and Ru/PILs-NTf_2 (ILs:EGDMA = 1:6, molar ratio) were chosen as the representative to characterize the physical and chemical properties of the supports and catalysts.

The FT-IR spectra presented in Fig. 1. It shows that all the samples exhibit an extremely broad and strong band at 2987–2963 cm^{-1}, which is attributable to stretching vibrations of the ν(C—H) group. Samples (a) and (b) presented several featured bands for imidazole, in which the bands at approximately 1649–1543 cm^{-1} were indicative of the imidazolium ring skeleton, whereas the band at 1457 cm^{-1} was attributed to the deformation vibration from the imidazole ring's ν(C—H) bond [33,34]. The observation of these bands supported the existence of imidazolium–IL moiety in the polymeric framework. The band at approximately 1723 cm^{-1}, which was attributable to ν(C═O) stretching vibration, was clearly observed on the spectra of the polymer (Fig. 1b) and EGDMA (Fig. 1c). The observation of these bands suggested the existence of EGDMA in the polymeric framework. The bands at approximately 3071 cm^{-1} and 3094 cm^{-1}, which were attributable to the unsaturated ν(C—H) vibrations, were clearly observed on the spectra of ILs (Fig. 1a) and EDGMA (Fig. 1c) but disappeared on the spectrum of the polymer (Fig. 1b), thereby demonstrating the consumption of the olefinic bond [22,35]. Therefore, polymerization can be regarded as complete. The vibration of ν(C═C) was not adopted for judgment due to the overlapping of this band with the vibration of ν(C═N), which complicated the FT-IR spectra. The results obtained from FT-IR were the same as those obtained from SEM. Hence, PILs that contained EGDMA and [EVIM]Br were concluded to be polymerized.

The SEM images (Fig. 2) show that the primary particles of PILs-Br are irregular, small particles at the nanometer level. They are tightly interacted and packed into large aggregates. Au/PILs-NTf_2 and Ru/PILs-NTf_2 present a similar morphology to PILs-Br. The elemental mapping analysis of PILs-Br demonstrated a relatively uniform dispersion of oxygen (O), nitrogen (N) and bromine (Br), thereby further verifying the existence of ILs and EGDMA in the network. These results are consistent with FT-IR patterns, which confirmed the polymerization of ILs and EGDMA. The elemental mapping analysis of Ru/PILs-NTf_2 and Au/PILs-NTf_2 demonstrated relatively uniform dispersion of sulfur (S) and fluorine (F), which further verified the existence of NTf_2 with

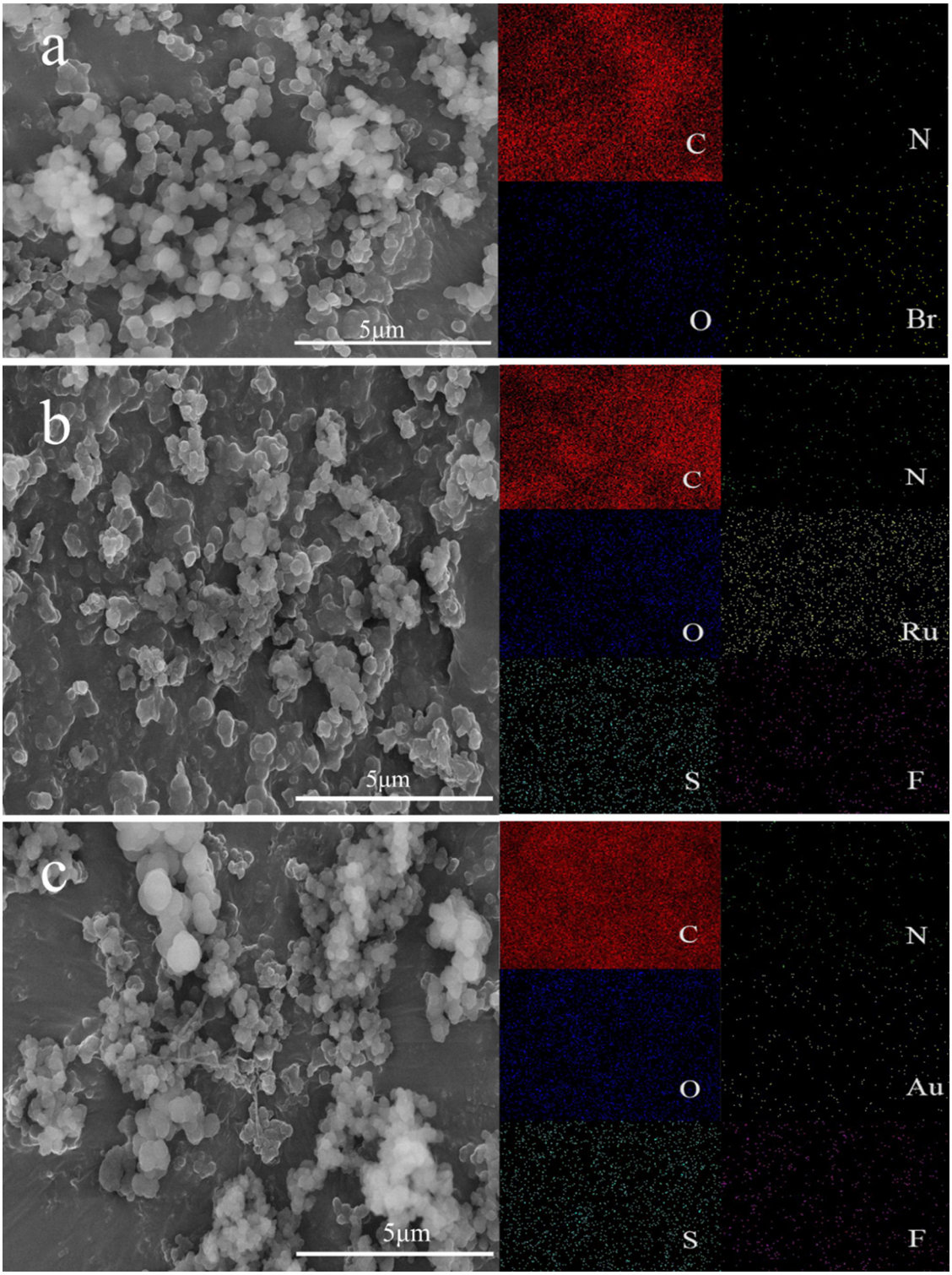

Fig. 2. SEM mapping analysis of C, N, O and Br elements on PILs-Br (a), C, N, O, Ru, S and F elements on Ru/PILs-NTf_2 (b) and C, N, O, Au, S and F elements on Au/PILs-NTf_2 (c).

the homogeneous distribution in the network and the successive immobilization of NTf_2 anions. In addition, the SEM elemental mapping images of Ru and Au showed their homogeneous distribution on the supports. This phenomenon is consistent with the XPS results. The −COO− group, −S═O group and the imidazole ring can interact with Au and Ru, respectively. Hence, NPs of Au and Ru can be uniformly distributed on the supports. The morphology, size, and distribution of the Ru or Au NPs on the support were further analyzed via TEM.

The TEM images of the supported catalysts and supports were shown in Fig. 3. The primary particles of the supports consist of nanospheres that are intertwined with one another to form a cross-linked framework, which is further confirmed by the TEM images, as shown in Fig. 3a. In the catalysts (Fig. 3b and c), Au was poorly dispersed and aggregated into large particles. The average size of the metal particles was 4.5 nm. Meanwhile, Ru exhibited better dispersion on the supports with an average size of 2.5 nm. Following the XPS results, Au can

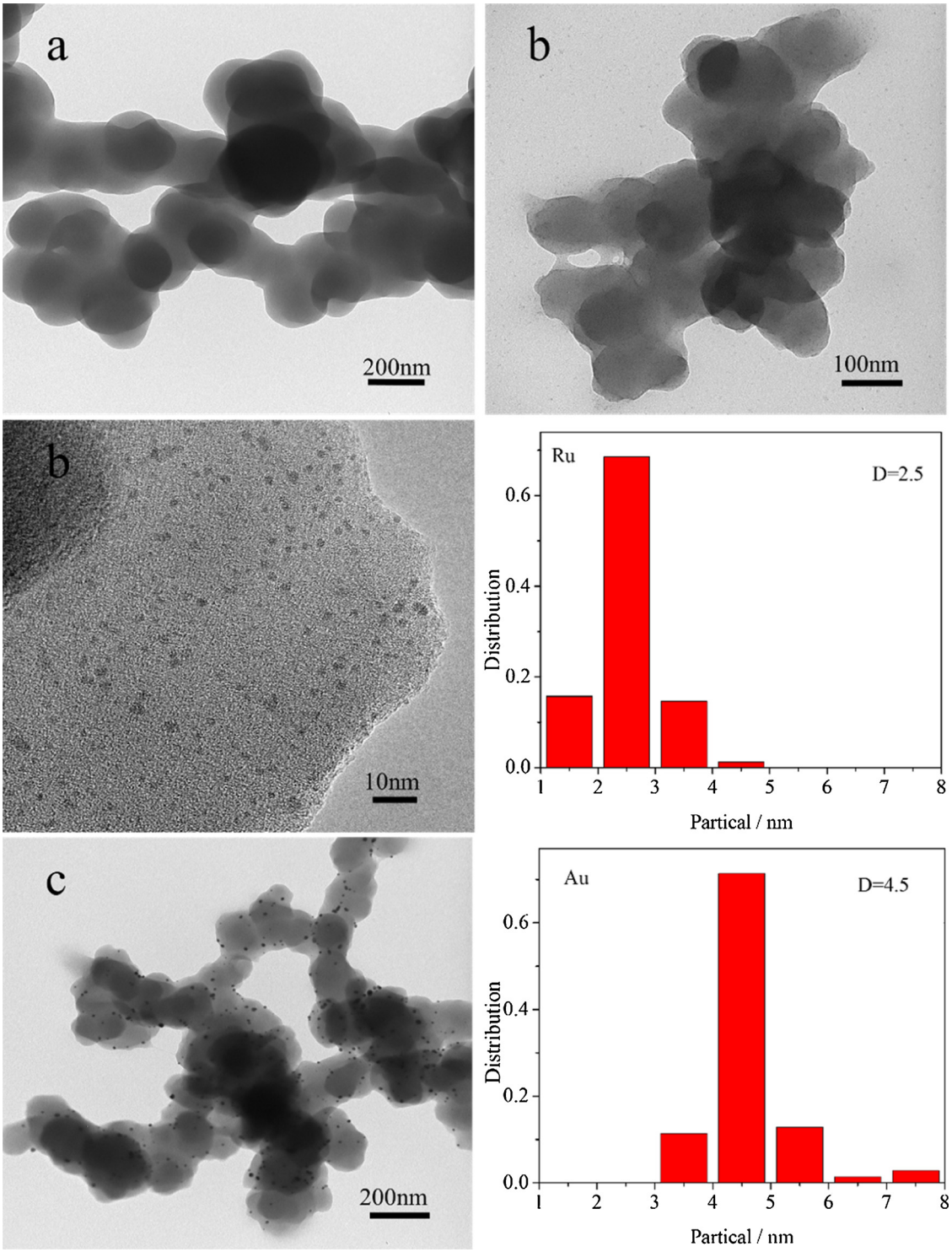

Fig. 3. (a) TEM image of PILs-NTf_2, (b) TEM image of Ru/PILs-NTf_2, (c) TEM image of Au/PILs-NTf_2.

simultaneously interact with the −COO− group (in EGDMA), −S═O group (in NTf_2) and imidazole ring of IL moieties, whereas Ru can only interact with the imidazole ring of IL moieties. Besides, the molar content of EGDMA in the support was approximately six times that of ILs. Hence, the interaction sites between Au and the support were considerably denser than that of Ru and the support, causing Au is more likely to aggregate larger NPs than Ru.

The XPS survey spectrum of the PILs-NTf_2, Au/PILs-NTf_2, and Ru/PILs-NTf_2 were showed in Figs. 4, 5 and 6 , respectively, and all the results were summarized in Table S2. In the N 1s XPS spectrum (Fig. 4A1) two peaks could be deconvoluted with the binding energy (BE) at 399.45 eV and 401.55 eV, which were assigned to pyrrolic and quaternary N, respectively [14,36,37]. The XPS spectrum of O 1s (Fig. 4B1) (C−O at 531.49 eV, S═O at 532.57, and C═O at 533.34 eV [38,39]) also confirmed the existence of O-containing groups. In Au/PILs-NTf_2, Au NPs were supported on PILs-NTf_2. Interestingly, O 1s BE was changed from 531.49, 532.57, and 533.34 eV to 531.43, 532.07, and 533.11 eV, respectively, which indicated that some of the electrons were transferred to O atoms. Meanwhile, N 1s BE was moved from 401.46 to 401.05 eV, which meant that some of the electrons were

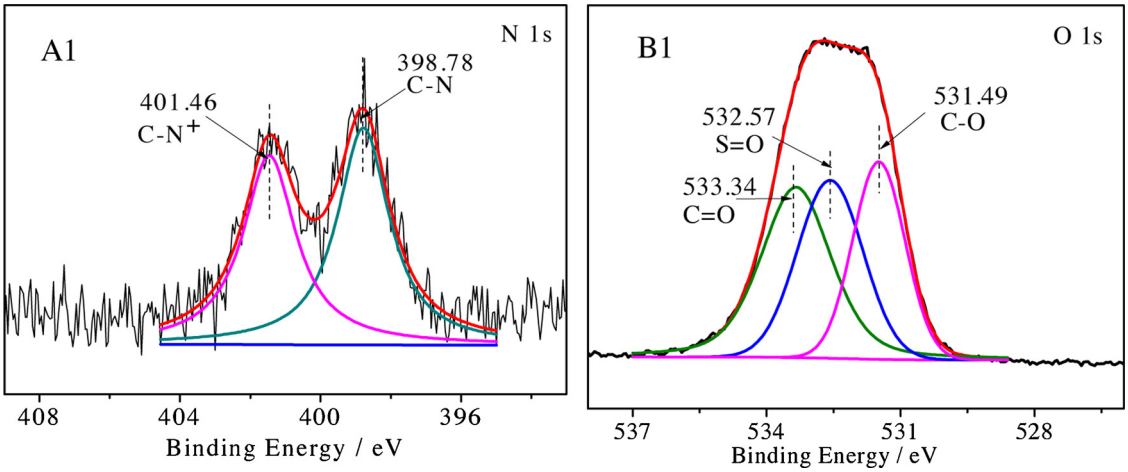

Fig. 4. (A1) N 1s XPS spectrum and (B1) O 1s XPS spectrum of the sample PILs-NTf_2.

transferred from Au^0 atom to N and O, thereby causing Au^{3+} species to be observed at 86.75 eV. A similar phenomenon was observed in Ru/PILs-NTf_2. For Ru/PILs-NTf_2, the most intensive photoemission line of Ru $3d_{5/2}$ overlapped with the C 1s line from the C support. Therefore, Ru surface species were investigated by analyzing the Ru $3p_{3/2}$ line, and the BE of $Ru\delta^+$ $3p_{3/2}$ was located at 462.46 eV. The BE of O 1s was nearly the same as that of PILs-NTf_2. However, the BE of N 1s was reduced by 0.25 eV, which suggested that some of the electrons were transferred from Ru particles. For Au/PILs-NTf_2, the N (in the imidazole ring) and the O (in the −COO− and −S═O group) can separately interact with Au. However, for Ru/PILs-NTf_2, only the N of the imidazole ring can interact with Ru. These interaction forces can stably and uniformly disperse metal NPs on the supports. Since the molar content of EGDMA in the supports was more than that of ILs, i.e., the interaction sites between Au and the support were considerably denser than that of between Ru and the support.

The TG analysis provided information related to the thermal stability of the PIL-NTf_2, Au/PILs-NTf_2, and Ru/PILs-NTf_2 specimens. Fig. 7 demonstrates that the decomposition temperature of PIL-NTf_2, Au/PILs-NTf_2, and Ru/PILs-NTf_2 are 298 °C, 305 °C, and 348 °C, respectively. It

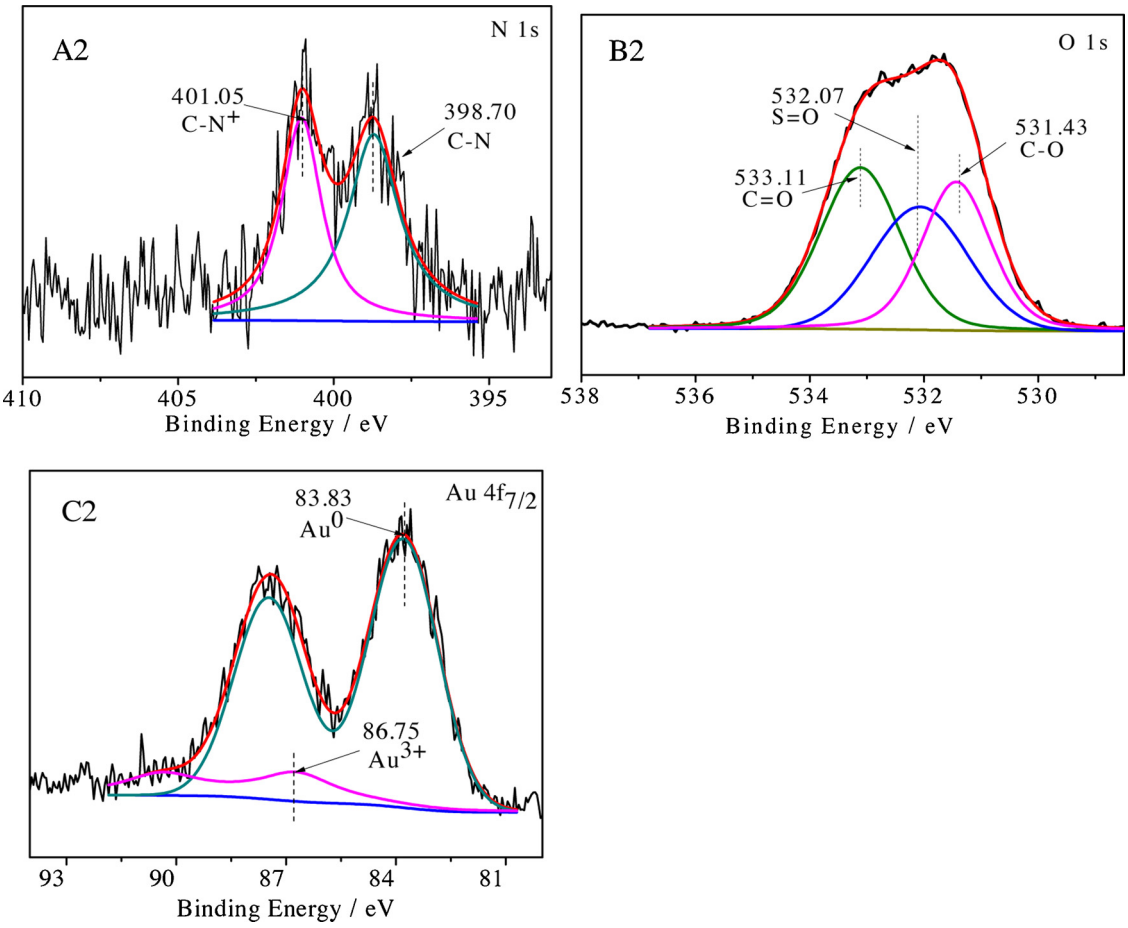

Fig. 5. (A2) N 1s XPS spectrum, (B2) O 1s XPS spectrum and (C2) Au $4f_{7/2}$ XPS spectrum of the sample Au/PILs-NTf_2.

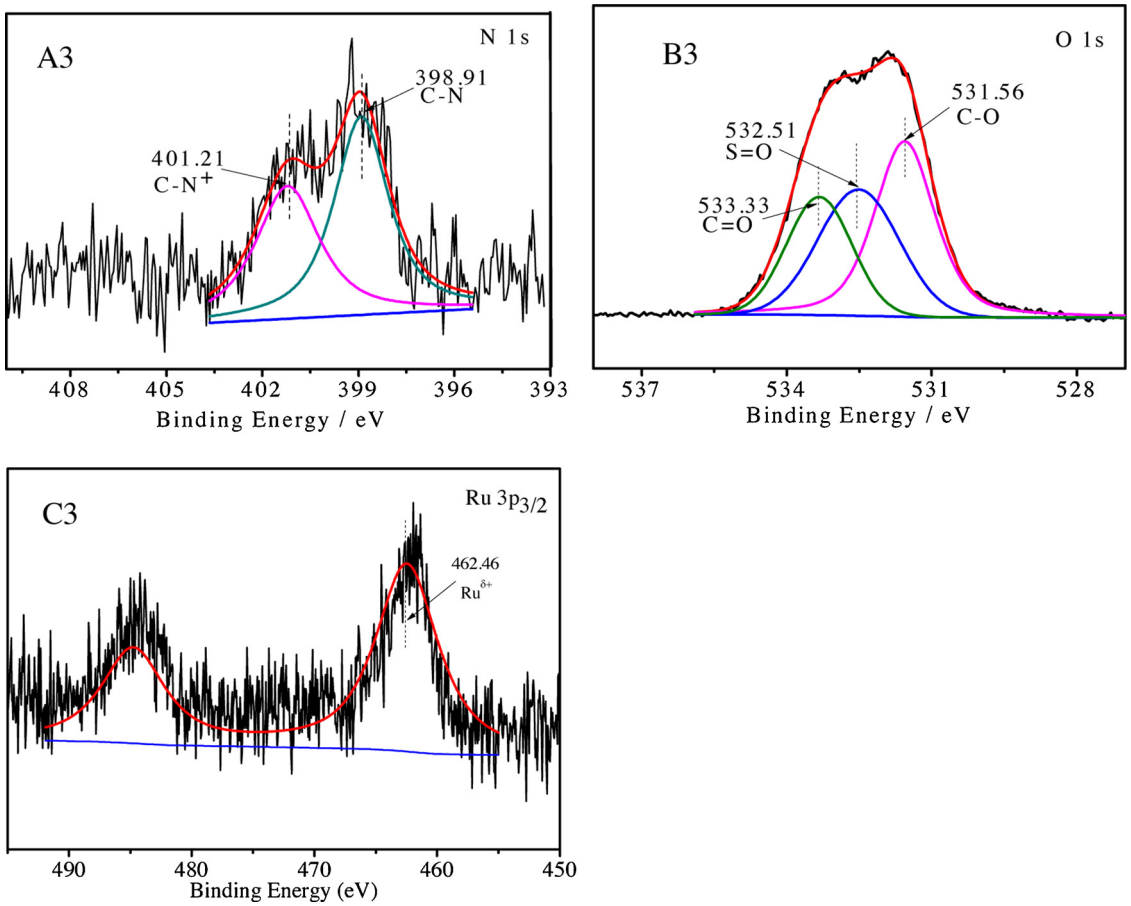

Fig. 6. (A3) N 1s XPS spectrum, (B3) O 1s XPS spectrum and (C3) Ru $3p_{3/2}$ XPS spectrum of the sample Ru/PILs-NTf_2.

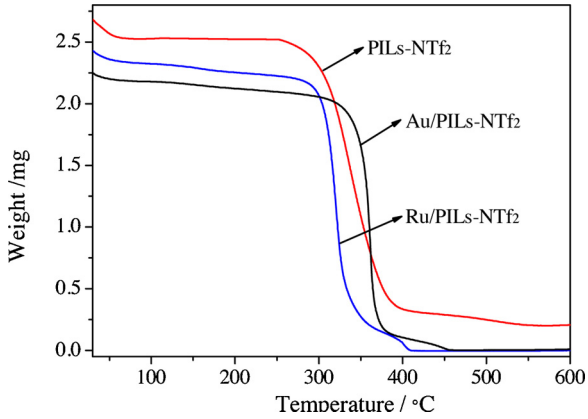

Fig. 7. The TG curves of PILs-NTf_2, Ru/PILs-NTf_2 and Au/PILs-NTf_2.

is noted that the decomposition temperatures of Au/PILs-NTf_2 and Ru/PILs-NTf_2 are higher than PIL-NTf_2. Therefore, the thermal stability of the catalyst is improved by the loading of active metals. Since the experimental temperatures are in the range from 140 to 180 °C in our proposed catalytic system, catalysts were thermally decomposed to affect the catalytic effect did not occur during the experiment.

3.2. Evaluation of catalyst performance in CWAO of ammonia

3.2.1. Structure of the support on catalytic performance

Fig. 8 illustrates the effects of the structure and content of ILs on the catalytic behavior of the Au/PILs-NTf_2 and Ru/PILs-NTf_2 catalysts, where temperature and pressure remained at 160 °C and 1 MPa, respectively. And the N-balance was recorded in Table S3. Moreover, Au/PILs-NTf_2 had a lower activity for the CWAO of ammonia than Ru/PILs-NTf_2 regardless of how the IL moieties in the polymer were adjusted. The Au/PILs-NTf_2 catalyst exhibited the advantage of excellent selectivity to N_2 (~99%), whereas the Ru/PILs-NTf_2 catalyst was less selective to N_2 than the Au/PILs-NTf_2 catalyst. In addition, the catalytic effect was affected by the molar ratio of ILs to EGDMA in the PIL backbone. The activity of the catalysts increased with the content of IL moieties in PILs within the range of 1:0~1:6 and decreased within the range of 1:6~1:2. On the one hand, the pore size and surface area of the supports can be influenced by the change in the molar ratio of ILs to EGDMA in the PIL backbone, thereby resulting in a change in catalytic effect. On the other hand, PILs can interact with the active metal, which facilitates the stable and uniform dispersion of the active metal on the supports, thereby affecting the activity of the catalyst. The former was analyzed via BET, whereas the latter was studied via XPS and TEM.

Table 2 shows that as the content of the IL moieties in PILs increased (the molar ratio of ILs and EGDMA from 1:10 to 1:2), S_{BET} decreases from 23.05 to 11.87 $m^2 g^{-1}$, and $V_p{}^b$ decreased from 0.06 to 0.03 $cm^3 g^{-1}$. The sharp decrease in S_{BET} and the $V_p{}^b$ were detrimental to the accumulation of reactants on the surface of the supports, particularly for O_2, which exhibited limited solubility in water. Adsorbing O_2 onto the supports is highly unfavorable. Hence, this phenomenon is extremely disadvantageous for the complete catalytic reaction. Following the XPS and TEM results, the interaction sites between four supports and the active metal could affect the uniformity of the distribution of the active metal on the supports.

Also, comparing the S_{BET} of the supports after loading the active center, it was found that S_{BET} changed greatly after loading Au (from 24.11–18.90 $cm^3 g^{-1}$), and the S_{BET} after loading Ru was not significantly changed. This phenomenon further proves the results of XPS

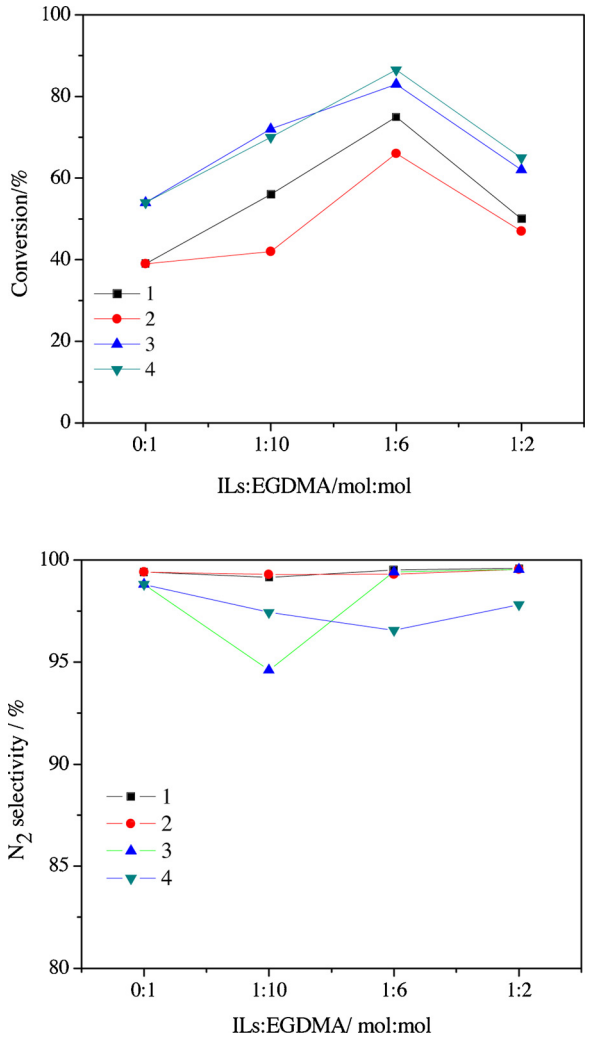

Fig. 8. Results of CWAO of ammonia over polymer supported metal catalysts at 160 °C under 1 MPa.1: Au/D-PILs-NTf_2, 2: Au/PILs-NTf_2, 3: Ru/D-PILs-NTf_2, 4: Ru/PILs-NTf_2.

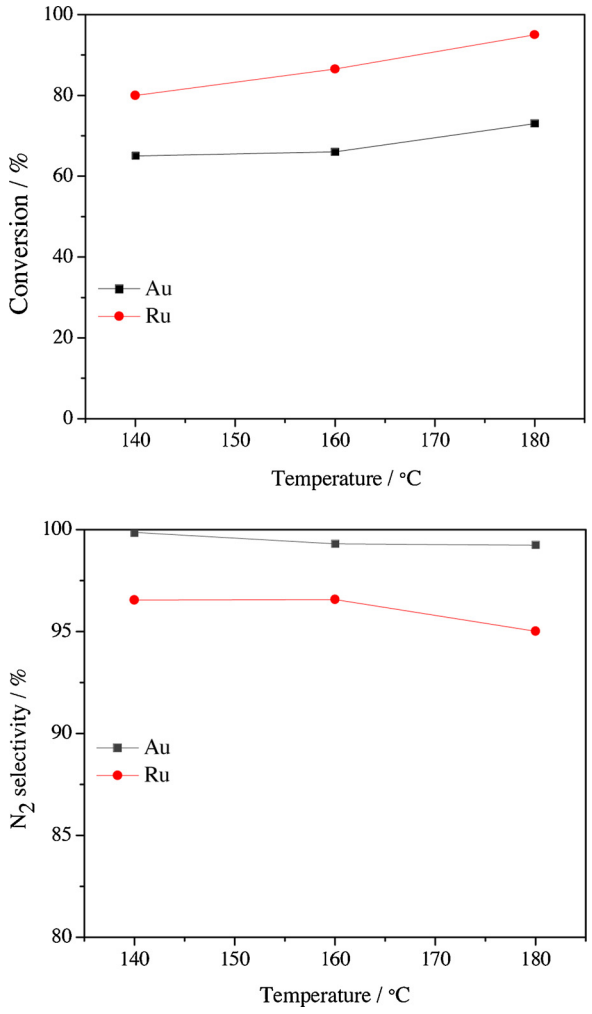

Fig. 9. Effect of reaction temperature on catalytic performance of Ru/PILs-NTf_2 and Au/PILs-NTf_2 catalysts. pH = 12, oxygen pressure = 1 MPa, reaction time = 4 h.

Table 2
The results of BET.

Entry	Support/Catalyst	ILs : EGDMA(mol)	S_{BET}[a] / $m^2 \cdot g^{-1}$	V_p[b] / $cm^3 \cdot g^{-1}$
1	PEGDMA	1:0	22.8	0.04
2	PILs-NTf_2	1:10	23.05	0.06
3	PILs-NTf_2	1:6	24.11	0.07
4	PILs-NTf_2	1:2	11.87	0.03
5	Au/PILs-NTf_2	1:6	18.90	0.05
6	Ru/PILs-NTf_2	1:6	22.85	0.06

[a] BET surface area.
[b] Total pore volume.

and TEM. According to the XPS analysis, the interaction sites between Au and the support are considerably denser than that of Ru, which causes Au more easily to aggregate on the support. This may block the channels of the support, resulting in a decrease of BET surface area of the Au/PILs.

3.2.2. Effects of temperature and pressure on the CWAO of ammonia

The Au/PILs-NTf_2 and Ru/PILs-NTf_2 catalysts were used to investigate the effects of temperature and pressure on catalytic performance and selectivity to N_2, the molar ratio of ILs to EGDMA was 1:6.

Three runs were conducted at different temperatures ranging from 140 to 180 °C, where the pressure was maintained at 1.0 MPa, the results were recorded in Fig. 9. And the N-balance was recorded in Tables S4 and S5. Fig. 9 illustrates that the Ru/PILs-NTf_2 catalyst is highly effective for the CWAO of ammonia, and the conversion can exceed 80% even at 140 °C. When the temperature increased from 140 to 180 °C, the conversion of the Au/PILs-NTf_2 catalyst was increased from 65% to 75% at these reaction temperatures. Although temperature enhanced the activity, the Au/PILs-NTf_2 catalyst maintained a better selectivity to N_2 within the entire range of the testing temperature.

The temperature was maintained at 150 °C, and the performance of the catalysts at pressures ranging from 1 to 2 MPa was shown in Fig. 10. And the N-balance was recorded in Tables S6 and S7. When the pressure changed from 1 to 2 MPa, the conversion of ammonia was maintained at approximately 70% under the catalyst of Au/PILs-NTf_2 and reached approximately 85% under the catalyst of Ru/PILs-NTf_2. Although the conversion of ammonia using Ru/PILs-NTf_2 as a catalyst was considerably higher than that using Au/PILs-NTf_2, the selectivity to N_2 of ammonia using Au/PILs-NTf_2 remained at approximately 99% with an increase in pressure. However, when pressure increased from 1 to 2 MPa, the selectivity to N_2 of ammonia using Ru/PILs-NTf_2 was decreased slightly.

By analyzing the influences of temperature and pressure on the performance of the CWAO of ammonia, the conversion of ammonia using PILs-supported Au or Ru has high activity and selectivity under milder condition. Regarding the activity of the Au/PILs-NTf_2 and Ru/

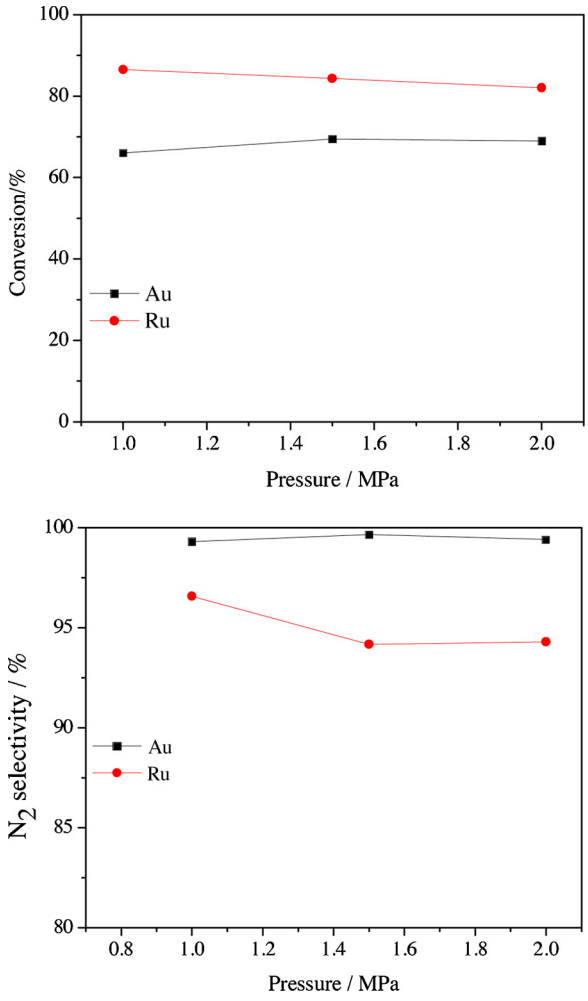

Fig. 10. Effect of oxygen pressure on catalytic performance of Au/PILs-NTf_2 and Ru/PILs-NTf_2 catalysts. pH = 12, temperature = 160 °C, reaction time = 4 h.

PILs-NTf_2, the lower activity of Au/PILs-NTf_2 compared to Ru/PILs-NTf_2 could then be ascribed to the smaller particle size as determined by TEM (Table S9), since the smaller particles are generally more active [40]. However, another factor may play an important role in the catalytic behavior, i.e. the different active metal supported on PILs. Generally, the activity of different metals to CWAO is different. It should be noted that the conversion of ammonia by Ru/PILs-NTf_2 was higher than that of Au/PILs-NTf_2 in the proposed catalytic system. Nevertheless, for selection to N_2, the Ru/PILs-NTf_2 catalyst was affected by temperature and pressure, whereas the Au/PILs-NTf_2 catalyst was hardly affected and achieved a higher selectivity to N_2 than the Ru/PILs-NTf_2 catalyst.

4. Catalyst stability determination

The stability of catalysts is an important parameter in practical applications and is perhaps more important than the activity of catalysts [41]. Given the Ru/PILs-NTf_2 catalyst could provide high conversion of ammonia and selectivity to N_2 at 160 °C and 1 MPa, the recycle experiments were operated by Ru/PILs-NTf_2, where the molar ratio of ILs to EGDMA was 1:6.

Recycling operations were applied to study stability under relatively mild conditions (160 °C and 1 MPa). When the first reaction was completed, the catalysts were recovered via filtration and dried for 24 h at 40 °C. Fig. 11 shows the different conversions of ammonia over 4 h in 3 cycle experiments. The Ru/PILs-NTf_2 catalyst showed excellent stability, and no deactivation was observed during the cyclic experiment.

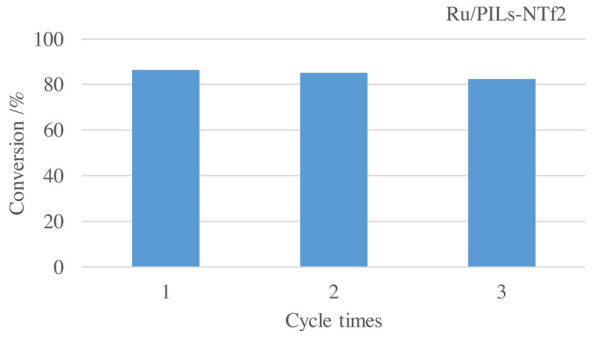

Fig. 11. Reusing effect of Ru/PILs-NTf_2 catalyst at 160 °C and 1 MPa.

Table 3
The leaching of Ru from PILs was analyzed by ICP-MS.

Catalyst	Cycle	Au or Ru leached (%)
Ru/PILs-NTf_2	1	2.9
Ru/PILs-NTf_2	2	3.3
Ru/PILs-NTf_2	3	3.7

The determination of the content of the active metal in the solution after the reaction using ICP-MS is a further exploration of the stability of the catalyst. Table 3 shows the measurement results of Ru content in solution after the above three cyclic reactions. A small amount of Ru NPs (˜3%) are leached from PILs-NTf_2 every run, leading to a slight decrease in the conversion of ammonia.

Based on the XPS results, the catalyst support could interact with the active metal (Ru) to promote the stable presence of active metal NPs on the supports. In addition, the TG analysis results showed that Ru/PILs-NTf_2 decomposed when the temperature exceeded 270 °C. Hence, at the test temperature (range from 160 to 180 °C), the catalyst would not be deactivated due to thermal decomposition. From the above points, a conclusion could be drawn that the catalysts used in the study achieved good stability.

5. Conclusion

In summary, Au/PILs and Ru/PILs were fabricated and employed as recyclable heterogeneous catalysts for the CWAO of ammonia. The results indicated that the Au/PILs and Ru/PILs catalysts with low active metal loadings performed efficiently under mild conditions. In this process, the imidazole ring, −COO− and −S═O groups could interact with the Au and Ru atoms, respectively, which could make the metal NPs stable and evenly dispersed on PILs. The results of the CWAO of ammonia indicated that 86.5% ammonia conversion with 95% selectivity to N_2 was obtained using Ru/PILs under 1 MPa at 160 °C in 4 h. In comparison, only 65.8% of conversion with a selectivity of 99% can be achieved when Au/PILs are applied. Moreover, the interactions between supports and metals could provide an excellent catalytic property for catalysts.

Declaration of Competing Interest

The authors declare that they have no known competing financial interests or personal relationships that could have appeared to influence the work reported in this paper.

Acknowledgments

We thank the support provided by the National Key R&D Program of China (No. 2017YFB0602804), the National Natural Science Foundation of China (No. 21878164).

Appendix A. Supplementary data

Supplementary material related to this article can be found, in the online version, at doi:https://doi.org/10.1016/j.apcatb.2019.117972.

References

[1] T.L. Huang, J.M. Macinnes, K.R. Cliffe, Nitrogen removal from wastewater by a catalytic oxidation method, Water Res. 35 (2001) 2113–2120.
[2] P.J. Riggan, R.N. Lockwood, E.N. Lopez, Deposition and processing of airborne nitrogen pollutants in Mediterranean-type ecosystems of southern California, Environ. Sci. Technol. 19 (1985) 781–789.
[3] A. Yadu, B.P. Sahariah, J. Anandkumar, Influence of COD/ammonia ratio on simultaneous removal of NH 4 + -N and COD in surface water using moving bed batch reactor, J. Water Process Eng. 22 (2018) 66–72.
[4] B. Liu, A. Giannis, J. Zhang, V.W.C. Chang, J.Y. Wang, Air stripping process for ammonia recovery from source-separated urine: modeling and optimization, J. Chem. Technol. Biot. 90 (2015) 2208–2217.
[5] P.H. Liao, A. Chen, K.V. Lo, Removal of nitrogen from swine manure wastewaters by ammonia stripping, Bioresour. Technol. 54 (1995) 17–20.
[6] G. Jeong, J.H. Jung, J.H. Lim, A computational mechanistic study of breakpoint chlorination for the removal of ammonia nitrogen from water, J. Chem. Eng. Jpn. 47 (2014) 225–229.
[7] T.A. Pressley, D.F. Bishop, S.G. Roan, Ammonia-nitrogen removal by breakpoint chlorination, Environ. Sci. Technol. 6 (1973) 622–628.
[8] Z. Xu, X. Dai, X. Chai, Effect of different carbon sources on denitrification performance, microbial community structure and denitrification genes, Sci. Total Environ. 634 (2018) 195–204.
[9] C. Fan, P. Wang, W. Zhou, S. Wu, S. He, J. Huang, L. Cao, The influence of phosphorus on the autotrophic and mixotrophic denitrification, Sci. Total Environ. 643 (2018) 127–133.
[10] J. Fu, K. Yang, C. Ma, N. Zhang, H. Gai, J. Zheng, B.H. Chen, Bimetallic Ru–Cu as a highly active, selective and stable catalyst for catalytic wet oxidation of aqueous ammonia to nitrogen, Appl. Catal. B-Environ. 184 (2016) 216–222.
[11] J. Qin, A.K. -I, Catalytic wet air oxidation of ammonia over alumina supported metals, Appl. Catal. B-Environ. 16 (1998) 261–268.
[12] S.D. Lin, A.C. Gluhoi, B.E. Nieuwenhuys, Ammonia oxidation over Au/MOx/γ-AlO—activity, selectivity and FTIR measurements, Catal. Today 85 (2004) 3–14.
[13] A. Taheri, B. Lai, C. Cheng, Y. Gu, Brønsted acid ionic liquid-catalyzed reductive Friedel–Crafts alkylation of indoles and cyclic ketones without using an external reductant, Green Chem. 17 (2015) 812–816.
[14] Q. Wang, W. Hou, S. Li, J. Xie, J. Li, Y. Zhou, J. Wang, Hydrophilic mesoporous poly (ionic liquid)-supported Au–Pd alloy nanoparticles towards aerobic oxidation of 5-hydroxymethylfurfural to 2,5-furandicarboxylic acid under mild conditions, Green Chem. 19 (2017) 3820–3830.
[15] Y. Liu, Y. Zhou, J. Li, Q. Wang, Q. Qin, W. Zhang, H. Asakura, N. Yan, J. Wang, Direct aerobic oxidative homocoupling of benzene to biphenyl over functional porous organic polymer supported atomically dispersed palladium catalyst, Appl. Catal. B-Environ. 209 (2017) 679–688.
[16] C.I. Ezugwu, M.A. Asraf, X. Li, S. Liu, C.-M. Kao, S. Zhuiykov, F. Verpoort, Selective and adsorptive removal of anionic dyes and CO2 with azolium-based metal-organic frameworks, J. Colloid Interface Sci. 519 (2018) 214–223.
[17] J. Yuan, H. Schlaad, C. Giordano, M. Antonietti, Double hydrophilic diblock copolymers containing a poly(ionic liquid) segment: controlled synthesis, solution property, and application as carbon precursor, Eur. Polym. J. 47 (2011) 772–781.
[18] D. Mecerreyes, Polymeric ionic liquids: broadening the properties and applications of polyelectrolytes, Prog. Polym. Sci. 36 (2011) 1629–1648.
[19] L. Wei, J. Liu, D. Zhao, Mesoporous materials for energy conversion and storage devices, Nat. Rev. Mater. 1 (2016) 16023.
[20] J.K. Sun, M. Antonietti, J. Yuan, Nanoporous ionic organic networks: from synthesis to materials applications, Chem. Soc. Rev. 45 (2016) 6627.
[21] Z. Wu, C. Chen, Q. Guo, B. Li, Y. Que, L. Wang, H. Wan, G. Guan, Novel approach for preparation of poly (ionic liquid) catalyst with macroporous structure for biodiesel production, Fuel 184 (2016) 128–135.
[22] C. Gao, G. Chen, X. Wang, J. Li, Y. Zhou, J. Wang, A hierarchical meso-macroporous poly(ionic liquid) monolith derived from a single soft template, Chem. Commun. 51 (2015) 4969–4972.
[23] M. Sun, S. Wang, Y. Li, H. Xu, Y. Chen, Promotion of catalytic performance by adding W into Pt/ZrO 2 catalyst for selective catalytic oxidation of ammonia, Appl. Surf. Sci. 402 (2017) 323–329.
[24] Z. Guo, Q. Jiang, Y. Shi, J. Li, X. Yang, W. Hou, Y. Zhou, J. Wang, Tethering dual hydroxyls into mesoporous poly(ionic liquid)s for chemical fixation of CO2 at ambient conditions: a combined experimental and theoretical study, ACS Catal. 7 (2017) 6770–6780.
[25] X. Wan, C. Zhou, J. Chen, Y. Yang, Y. Wang, W. Deng, Q. Zhang, Base-free aerobic oxidation of 5-hydroxymethyl-furfural to 2,5-Furandicarboxylic acid in water catalyzed by functionalized carbon nanotube-supported Au–Pd alloy nanoparticles, ACS Catal. 4 (2014) 2175–2185.
[26] Y. Liu, W. Kai, H. Wei, W. Shan, L. Jing, Z. Yu, J. Wang, Mesoporous poly(ionic liquid) supported palladium(II) catalyst for oxidative coupling of benzene under atmospheric oxygen, Appl. Surf. Sci. 427 (2018) S0169433217323425.
[27] L. Dagang, Z. Yi, L. Zehui, T. Donglin, C. Lei, C. Peng, Chitin nanofibrils for rapid and efficient removal of metal ions from water system, Carbohyd. Polym. 98 (2013) 483–489.
[28] H. Song, Z. Na, C. Zhong, L. Zong, X. Meng, H. Gai, Hydrogenation of CO2 into formic acid over palladium catalyst on chitin, New J. Chem. 41 (2017) 9170–9177.
[29] X.-d. Mu, J.-q. Meng, Z.-C. Li, Y. Kou, Rhodium nanoparticles stabilized by ionic copolymers in ionic liquids: long lifetime nanocluster catalysts for benzene hydrogenation, J. Am. Chem. Soc. 127 (2005) 9694–9695.
[30] C. Pavia, E. Ballerini, L.A. Bivona, F. Giacalone, C. Aprile, L. Vaccaro, M. Gruttadauria, Palladium supported on cross-linked imidazolium network on silica as highly sustainable catalysts for the suzuki reaction under flow conditions, Adv. Synth. Catal. 355 (2013) 2007–2018.
[31] X. Lu, Y. Yang, Y. Zeng, L. Li, X. Wu, Rapid and reliable determination of p-nitroaniline in wastewater by molecularly imprinted fluorescent polymeric ionic liquid microspheres, Biosens. Bioelectron. 99 (2017) 47–55.
[32] D.K. Lee, Mechanism and kinetics of the catalytic oxidation of aqueous ammonia to molecular nitrogen, Environ. Sci. Technol. 37 (2003) 5745–5749.
[33] P. Yan, Z. Gongbing, L. Nguyen, Z. Baoning, Q. Minghua, T. Franklin Feng, Synthesis and catalysis of chemically reduced metal-metalloid amorphous alloys, Chem. Soc. Rev. 41 (2012) 8140–8162.
[34] X. Zhao, L. Ma, Y. Yan, D. Yi, X. Shen, Ti2Ni alloy: a potential candidate for hydrogen storage in nickel/metal hydride secondary batteries, Energy Environ. Sci. 3 (2010) 1316–1321.
[35] L. Peng, J. Zhang, S. Yang, B. Han, X. Sang, C. Liu, G. Yang, Porosity control in mesoporous polymers using CO2-swollen block copolymer micelles as templates and their use as catalyst supports, Chem. Commun. 50 (2014) 11957–11960.
[36] H. Gai, K. Guo, M. Xiao, N. Zhang, Z. Li, Z. Lv, H. Song, Ordered mesoporous carbons as highly efficient absorbent for coal gasification wastewater – a real case study based on the Inner Mongolia autonomous coal gasification wastewater, Chem. Eng. J. 341 (2018) 471–482.
[37] Z. Ma, H. Zhang, Z. Yang, G. Ji, B. Yu, X. Liu, Z. Liu, Mesoporous nitrogen-doped carbons with high nitrogen contents and ultrahigh surface areas: synthesis and applications in catalysis, Green Chem. 18 (2016) 1976–1982.
[38] Y. Lin, X. Pan, W. Qi, B. Zhang, D.S. Su, Nitrogen-doped onion-like carbon: a novel and efficient metal-free catalyst for epoxidation reaction, J. Mater. Chem. A 2 (2014) 12475–12483.
[39] S. Marek, S. Martin, H. Markus, M. Florian, S. Hans-Peter, P. Natalia, W. Peter, L. Mathias, G.J. Michael, Ionic liquid based model catalysis: interaction of [BMIM][Tf2N] with Pd nanoparticles supported on an ordered alumina film, Phys. Chem. Chem. Phys. 12 (2010) 10610–10621.
[40] H. Ait Rass, N. Essayem, M. Besson, Selective aqueous phase oxidation of 5-hydroxymethylfurfural to 2,5-furandicarboxylic acid over Pt/C catalysts: influence of the base and effect of bismuth promotion, Green Chem. 15 (2013) 2240.
[41] J.W. Yoon, T.U. Yoon, E.J. Kim, A.R. Kim, T.S. Jung, S.S. Han, Y.S. Bae, Highly selective adsorption of CO over CO2 in a Cu(I)-chelated porous organic polymer, J. Hazard. Mater. 341 (2018) 321–327.